Confronting Braneworld Cosmology with Supernova data and Baryon Oscillations

Ujjaini Alam[a,b] and Varun Sahni[a]

[a] *Inter-University Centre for Astronomy and Astrophysics,*

Post Bag 4, Ganeshkhind

Pune 411 007, India and

[b]*International Centre for Theoretical Physics,*

Strada Costiera 11, 34100 Trieste, Italy

Abstract

Braneworld cosmology has several attractive and distinctive features. For instance the effective equation of state in braneworld models can be both quintessence-like ($w_0 \geq -1$) as well as phantom-like ($w_0 \leq -1$). Models with $w_0 \geq -1$ ($w_0 \leq -1$) are referred to as Brane 2 (Brane 1) and correspond to complementary embeddings of the brane in the bulk. (The equation of state in Brane 1 can successfully cross the 'phantom divide' at $w = -1$.) In this paper we compare the predictions of braneworld models to two recently released supernova data sets: the 'Gold' data (Riess *et al.*, 2004) and the data from the Supernova Legacy Survey (SNLS) (Astier *et al.*, 2005). We also incorporate the recent discovery of the baryon acoustic peak in the Sloan Digital Sky Survey (Eisenstein *et al.*, 2005) into our analysis. Our main results are that braneworld models satisfy both sets of SNe data. Brane 1 (with $w_0 \leq -1$) shows very good agreement with data for values of the matter density bounded *from below*: $\Omega_{0m} \gtrsim 0.25$ (Gold) and $\Omega_{0m} \gtrsim 0.2$ (SNLS). On the other hand Brane 2 (with $w_0 \geq -1$) shows excellent agreement with data for values of the matter density which are bounded *from above*: $\Omega_{0m} \lesssim 0.45$ (Gold) and $\Omega_{0m} \lesssim 0.35$ (SNLS). The DGP model is excluded at 3σ by SNLS and at 1σ by the Gold dataset. Braneworld models with future 'quiescent' singularities (at which the Hubble parameter and the matter density remain finite but higher derivatives of the expansion factor diverge) are excluded by both datasets.

INTRODUCTION

One of the most remarkable discoveries of the past decade has been the observation that the expansion of the universe is speeding up rather than slowing down. The case for an accelerating universe was first made on the basis of high redshift type Ia supernovae [1, 2, 3], and has since received support from deeper and better quality SNe data [4, 5, 6, 7, 9] as well as observations of the cosmic microwave background and large scale structure [10, 11].

Theoretically, an accelerating universe can be constructed in a number of distinct ways (see [12] and references therein). However three approaches have received considerable attention in the literature, these are:

- *The cosmological constant.* The acceleration of the universe is caused by the cosmological constant which satisfies $T_{ik} = \Lambda g_{ik}$ and, hence, has an equation of state $p = -\rho$. The combination of a Λ-term and cold dark matter results in the ΛCDM model which appears to provide excellent agreement with cosmological observations and, when combined with inflationary predictions of an (almost) scale invariant spectrum of density perturbations, comprises what may be called the 'standard model of cosmology'.

  However, despite its long and chequered history (since its inception by Einstein in 1917), a firm theoretical basis for a small Λ-term has so far eluded researchers [13]. Indeed, the value of the cosmological constant predicted by quantum field theory is at least 10^{55} times larger than its observed value $\rho_{\rm vac} = \Lambda/8\pi G \simeq 10^{-47} {\rm GeV}^4$, indicated by recent observations. This fact, taken together with the unevolving nature of Λ, suggests that the present epoch may be quite special since $\Omega_\Lambda \simeq 2\Omega_{\rm 0m}$. The resulting *cosmic coincidence* and the high degree of fine tuning associated with a small Λ-term have lead physicists to look for alternatives to the cosmological constant hypothesis.

- *Dark Energy.* The expansion of the universe is governed by the field equations of general relativity (GR), but one (or more) components of 'matter' violate the strong energy condition (SEC) $\rho + 3p \geq 0$ thereby causing the universe to accelerate. To this category belong quintessence models, the Chaplygin gas, topological defects and numerous other models of dark energy. In general, dark energy can be characterized by an equation of state $w = p/\rho$, where the observationally determined value of w can be used to constrain parameters of a given dark energy model. Although most

DE models have $w \neq$ constant some might say that the cosmological constant with $w = -1$ also belongs to this category.

- *Geometric approaches to acceleration.* The late-time acceleration of the universe is caused by a departure of space-time physics from standard GR on large scales and/or at late times. An important example of this class of models is braneworld cosmology according to which our three dimensional universe is a lower dimensional 'brane' embedded in a higher dimensional 'bulk' space-time. Braneworld models may provide a low energy manifestation of string/M-theory [14, 15]. Within the cosmological context braneworld models provide exciting new possibilities some of which are summarized below (also see [16]).

(i) 'Quintessential Inflation' [17] based on the Randall-Sundrum (RS) model [15] may provide a compelling explanation of both early and late-time acceleration within a single unified setting [18]. (ii) The Dvali-Gabadadze-Porrati (DGP) model can lead to an accelerating universe without the presence of a cosmological constant or some other form of dark energy [19, 20]. (iii) A family of braneworld models [22] which unify the approaches of RS and DGP allow the *effective* equation of state of dark energy to be 'quintessence-like' $w \geq -1$ as well as 'phantom-like' $w < -1$. In a subclass of these models the acceleration of the universe is a *transient* phenomenon, which gives way to matter dominated expansion in the future. The absence of horizons in a transiently accelerating space-time is an attractive feature of this scenario since it can reconcile current observations of acceleration with the demands of string/M-theory [23]. (iv) Another aspect of the braneworld cosmology [22] is the possibility of fundamentally new cosmological behaviour (*loitering* [24] & *mimicry* [25]) at moderately high redshifts. Loitering and mimicry models remain close to ΛCDM in the future (hence providing excellent agreement with SNe data) while departing from ΛCDM-like behaviour in the past. The older age of these braneworld models might make them better equipped to explain the existence of high redshift QSO's and also allow for a lower redshift of reionization than that predicted in ΛCDM cosmology [26, 27, 28, 29].

Whether the increasingly large number of low and high redshift observations can be accommodated within the braneworld paradigm is an important subject demanding extensive exploration. Our purpose in this paper will be more modest, we shall examine the

braneworld models proposed in [22] in the light of the Gold SNe data set [7] and the 71 new SNe discovered by the Supernova Legacy Survey [9]. We shall use this data in conjunction with the recent discovery of the baryon acoustic peak in the Sloan Digital Sky Survey [30] to place constraints on the parameter space of accelerating braneworld models. An outline of our paper is as follows: in section II we briefly describe braneworld cosmology, while section III is devoted to testing braneworld against observations. Our results and conclusions are presented in section IV.

ACCELERATING BRANEWORLD UNIVERSE

The equations of motion governing the braneworld can be derived from the action [31, 32]

$$S = M^3 \left[\int_{\text{bulk}} (R_5 - 2\Lambda_{\text{b}}) - 2 \int_{\text{brane}} K \right] + \int_{\text{brane}} \left(m^2 R_4 - 2\sigma \right) + \int_{\text{brane}} L \left(h_{\alpha\beta}, \phi \right) . \quad (1)$$

Here, R_5 is the scalar curvature of the metric g_{ab} in the five-dimensional bulk, and R_4 is the scalar curvature of the induced metric $h_{\alpha\beta}$ on the brane. The quantity $K = K_{\alpha\beta} h^{\alpha\beta}$ is the trace of the extrinsic curvature $K_{\alpha\beta}$ on the brane defined with respect to its *inner* normal. $L(h_{\alpha\beta}, \phi)$ is the four-dimensional matter field Lagrangian, M and m denote, respectively, the five-dimensional and four-dimensional Planck masses, Λ_{b} is the bulk cosmological constant, and σ is the brane tension. Integrations in (1) are performed with respect to the volume elements on the bulk and brane.

The action (1) presents a synthesis of the higher-dimensional ansatzes proposed by Randall and Sundrum [15] and Dvali, Gabadadze, and Porrati [19]. An important role in (1) is played by the $m^2 \int R_4$ term. This term was first introduced by Sakharov in a seminal paper [21] to describe the backreaction of quantum fluctuations of matter fields (which, in our case, reside on the brane). Its presence is crucial in making the braneworld accelerate since it introduces an important length scale

$$\ell = 2m^2/M^3 .$$

On short length scales $r \ll \ell$ (early times) one recovers general relativity, whereas on large length scales $r \gg \ell$ (late times) brane-specific effects begin to play an important role, leading to the acceleration of the universe [19, 22].

The cosmological evolution of a spatially flat braneworld is described by the Hubble

4

parameter

$$H^2(a) = \frac{A}{a^3} + B + \frac{2}{\ell^2}\left[1 \pm \sqrt{1 + \ell^2\left(\frac{A}{a^3} + B - \frac{\Lambda_{\mathrm{b}}}{6} - \frac{C}{a^4}\right)}\right] \, , \tag{2}$$

where

$$A = \frac{\rho_0 a_0^3}{3m^2} \, , \quad B = \frac{\sigma}{3m^2} \, , \tag{3}$$

and the 'dark radiation' term C/a^4 describes the projection of bulk degrees of freedom onto the brane. (Note that the four-dimensional Planck mass m is related to the effective Newton's constant on the brane as $m = 1/\sqrt{8\pi G}$.)

The two signs in (2) correspond to the two distinct ways in which the brane can be embedded in the higher dimensional bulk. Three limiting cases of our model may be of interest to the reader:

1. $m = 0$ in (2) corresponds to the well known FRW generalization of the RS scenario

$$H^2 + \frac{\kappa}{a^2} = \frac{\Lambda_{\mathrm{b}}}{6} + \frac{C}{a^4} + \frac{(\rho + \sigma)^2}{9M^6} \, . \tag{4}$$

2. $M = 0$ in (2) gives rise to ΛCDM

$$H^2(a) = \frac{A}{a^3} + B \, . \tag{5}$$

3. Finally, by setting $\sigma = 0$ and $\Lambda_{\mathrm{b}} = 0$ in (2) we recover the DGP model [19].

The Braneworld models proposed in [22] fall into two main categories:

- **Brane 1** (B1): The lower sign in (2) leads to the following form of the Hubble parameter [40]:

$$H^2(a) = \frac{A}{a^3} + \Lambda_{\mathrm{eff}} \, . \tag{6}$$

The effective cosmological 'constant' Λ_{eff} is composed of two terms: a constant Λ-term and a 'screening term' [33]:

$$\Lambda_{\mathrm{eff}} = \underbrace{(B + \frac{2}{\ell^2})}_{} - \underbrace{\frac{2}{\ell^2}\sqrt{1 + \ell^2\left(\frac{A}{a^3} + B - \frac{\Lambda_b}{6}\right)}}_{} \tag{7}$$

$$\Downarrow \qquad\qquad\qquad\qquad \Downarrow \tag{8}$$

$$\Lambda \qquad\qquad\qquad \text{Screening term}$$

Since the screening term decreases with time, the value of *the effective cosmological constant* Λ_{eff} *increases*. In this respect Brane 1 resembles phantom cosmology which has $w < -1$. It is important to note, however, that in the braneworld case there is *no violation of the weak energy condition and also no future 'big rip' singularity*. Indeed, from (7) it is quite clear that the universe evolves to ΛCDM in the future.

Since our main desire in this paper will be to test braneworld models against observations, it will be helpful to recast Eq. (2) with the lower sign in the following form

$$\frac{H^2(z)}{H_0^2} = \Omega_{0\text{m}}(1+z)^3 + \Omega_\sigma + \underline{2\Omega_\ell - 2\sqrt{\Omega_\ell}\sqrt{\Omega_{0\text{m}}(1+z)^3 + \Omega_\sigma + \Omega_\ell + \Omega_{\Lambda_{\text{b}}}}} , \quad (9)$$

where $z = a_0/a(t) - 1$ is the cosmological redshift, while

$$\Omega_{0\text{m}} = \frac{\rho_0}{3m^2 H_0^2} , \quad \Omega_\sigma = \frac{\sigma}{3m^2 H_0^2} , \quad \Omega_\ell = \frac{1}{l^2 H_0^2} , \quad \Omega_{\Lambda_{\text{b}}} = -\frac{\Lambda_{\text{b}}}{6H_0^2} , \quad (10)$$

are dimensionless parameters whose values must be determined from observations. Ω_σ is determined by the constraint relation

$$\Omega_{0\text{m}} + \Omega_\sigma - \underline{2\sqrt{\Omega_\ell}\sqrt{1 + \Omega_{\Lambda_{\text{b}}}}} = 1. \quad (11)$$

The difference between ΛCDM and braneworld cosmology is brought about by the underlined terms in (9) & (11).

- **Brane 2** (B2): The upper sign in (2) results in

$$\frac{H^2(z)}{H_0^2} = \Omega_{0\text{m}}(1+z)^3 + \Omega_\sigma + \underline{2\Omega_\ell + 2\sqrt{\Omega_\ell}\sqrt{\Omega_{0\text{m}}(1+z)^3 + \Omega_\sigma + \Omega_\ell + \Omega_{\Lambda_{\text{b}}}}} , \quad (12)$$

where $\Omega_\ell < 1 + \Omega_{\Lambda_{\text{b}}}$ and Ω_σ is determined from

$$\Omega_{0\text{m}} + \Omega_\sigma + \underline{2\sqrt{\Omega_\ell}\sqrt{1 + \Omega_{\Lambda_{\text{b}}}}} = 1. \quad (13)$$

The difference between ΛCDM and braneworld cosmology is brought about by the underlined terms in (12) & (13).

The two models Brane 1 and Brane 2 are complementary and reflect the two distinct ways in which the brane can be embedded in the bulk.

From (9) & (12) it is easy to see that both braneworld models approach the standard matter dominated universe at early times [with a small correction term $\sim (1 + z)^{3/2}$].

6

At late times the behaviour of the braneworld can differ from both ΛCDM and SCDM. This feature makes braneworld models testable and allows the braneworld scenario to provide a new explanation for the observational discovery of an accelerating universe. The expansion of the braneworld can be characterized by the deceleration parameter

$$q(z) = \frac{H'(z)}{H(z)}(1+z) - 1\,, \tag{14}$$

and the *effective* equation of state

$$w(z) = \frac{2q(z) - 1}{3\left[1 - \Omega_{\mathrm{m}}(z)\right]}\,. \tag{15}$$

From (9), (12), (14) and (15) it is easy to obtain the following expression for the current value of the effective equation of state [22]

$$w_0 = -1 \pm \frac{\Omega_{\mathrm{0m}}}{1 - \Omega_{\mathrm{0m}}}\sqrt{\frac{\Omega_\ell}{\Omega_{\mathrm{0m}} + \Omega_\sigma + \Omega_\ell + \Omega_{\Lambda_{\mathrm{b}}}}}\,, \tag{16}$$

and we immediately find that $w_0 \leq -1$ when we take the lower sign in (16), which corresponds[41] to Brane 1. The second choice (Brane 2) gives $w_0 \geq -1$.

- *Mimicry models.* It is interesting to note that for values of z and $\Omega_{\Lambda_{\mathrm{b}}}$ & Ω_ℓ satisfying

$$\Omega_{\mathrm{0m}}(1+z)^3 \ll \left(\sqrt{1 + \Omega_{\Lambda_{\mathrm{b}}}} \mp \sqrt{\Omega_\ell}\right)^2\,, \tag{17}$$

Eqs. (9) and (12) reduce to

$$\frac{H^2(z)}{H_0^2} \simeq \Omega_{\mathrm{m}}^{\Lambda\mathrm{CDM}}(1+z)^3 + 1 - \Omega_{\mathrm{m}}^{\Lambda\mathrm{CDM}}\,, \tag{18}$$

where the new density parameter $\Omega_{\mathrm{m}}^{\Lambda\mathrm{CDM}}$ is defined by the relation

$$\Omega_{\mathrm{m}}^{\Lambda\mathrm{CDM}} = \frac{\alpha}{\alpha \mp 1}\Omega_{\mathrm{m}}\,, \quad \alpha = \frac{\sqrt{1 + \Omega_{\Lambda_{\mathrm{b}}}}}{\sqrt{\Omega_\ell}}\,. \tag{19}$$

The braneworld therefore displays a remarkable property called *"cosmic mimicry"*: at low redshifts, the Brane 1 universe expands as ΛCDM (18) with $\Omega_{\mathrm{m}}^{\Lambda\mathrm{CDM}} < \Omega_{\mathrm{m}}$ [$\Omega_{\mathrm{m}}^{\Lambda\mathrm{CDM}}$ is determined by (19) with the lower ("+") sign]. The Brane 2 model at low redshifts also mimics ΛCDM but with a *larger value* of the density parameter $\Omega_{\mathrm{m}}^{\Lambda\mathrm{CDM}} > \Omega_{\mathrm{m}}$ with $\Omega_{\mathrm{m}}^{\Lambda\mathrm{CDM}}$ being determined by (19) with the upper ("−") sign.

The range of redshifts over which cosmic mimicry occurs is given by $0 \leq z \ll z_{\mathrm{m}}$, where

$$z_{\mathrm{m}} = \frac{\left(\sqrt{1 + \Omega_{\Lambda_{\mathrm{b}}}} \mp \sqrt{\Omega_{\ell}}\right)^{2/3}}{\Omega_{0\mathrm{m}}^{1/3}} - 1 \,. \tag{20}$$

As demonstrated in [25] the Hubble parameter in mimicry models departs from that in ΛCDM at *intermediate* redshifts ($z > z_{\mathrm{m}} \sim$ few). This could lead to interesting cosmological effects since the age of the high redshift universe in a mimicry model can be greater than that in ΛCDM while the redshift of reionization can be lower [25]. Since the mimicry models and ΛCDM are virtually indistinguishable at lower redshifts, both are expected to fit the SNe data (at $z < 2$) equally well.

COMPARING BRANEWORLD MODELS WITH OBSERVATIONS

In this paper we shall compare the braneworld model [22] against three sets of observations. We briefly summarize each of the data sets which we shall use before proceeding to give the results of our comparison.

1. *The Gold SNe data set* : As recently as 2003, the entire supernova dataset from the two different surveys – Supernova Cosmology Project (SCP) and High z Supernova Search Team (HZT), along with low redshift supernovae from Calan-Tololo Supernova Search (CTSS) comprised of a meager 92 supernovae [1, 1, 2], with very few at high redshifts, $z > 0.7$. The method of data reduction for the different teams was also somewhat different, so that it was not possible to use the supernovae from the two datasets concurrently. The picture changed somewhat dramatically during 2003-2004, when a set of papers from both these teams [4, 5, 6] presented a joint dataset of 194 supernovae which used the same data reduction method. This new data resulted in doubling the dataset at $z > 0.7$. Not all these supernovae could be identified beyond doubt as Type Ia supernovae however, in many cases complete spectral data was not available. In early 2004, Riess *et al.*[7] reanalyzed the data with somewhat more rigorous standards, excluding several supernovae for uncertain classification or inaccurate colour measurements. They also added 14 new high redshift supernovae observed by the Hubble Space Telescope (HST) to this sample. The resultant sample comprises of 157 supernovae (the furthest being at redshift $z = 1.75$) which have been

classified as Type Ia supernovae beyond doubt– the 'Gold' dataset. We shall be using this 'Gold' dataset as our first supernova sample.

2. *The Supernova Legacy Survey SNe data set (SNLS)* : The SuperNova Legacy Survey [8] is an ongoing 5-year project which is expected to yield more than 700 spectroscopically confirmed supernovae below redshift of one. The first year results from this survey [9] have provided us with 71 new supernovae below $z = 1$. We shall use these 71 SNe together with the already available low-z supernova data, *ie* a total of 115 SNe, as our second supernova sample.

3. *The Baryon Acoustic Oscillation Peak (BAO)* : A remarkable confirmation of the standard big bang cosmology has been the recent detection of a peak in the correlation function of luminous red galaxies in the Sloan Digital Sky Survey [30]. This peak, which is predicted to arise precisely at the measured scale of 100 h^{-1} Mpc due to acoustic oscillations in the primordial baryon-photon plasma prior to recombination, can provide a 'standard ruler' with which to test dark energy models. Specifically, we shall use the value [30]

$$A = \frac{\sqrt{\Omega_{0m}}}{h(z_1)^{1/3}} \left[\frac{1}{z_1} \int_0^{z_1} \frac{dz}{h(z)} \right]^{2/3} = 0.469 \pm 0.017 \ , \tag{21}$$

where $h(z) = H(z)/H_0$ is defined in (9) and (12) for Brane 1 and Brane 2 respectively, and $z_1 = 0.35$ is the redshift at which the acoustic scale has been measured.

Methodology and Results

For the supernova data, we shall use the χ^2 minimization where

$$\chi^2(H_0, \Omega_{0m}, p_j) = \sum_i \frac{[y_{\text{fit},i}(z_i; H_0, \Omega_{0m}, p_j) - y_i]^2}{\sigma_i^2} \ . \tag{22}$$

Here, y_i is the data at redshift of z_i and σ_i is the uncertainty in the individual y_i, and p_j are the braneworld parameters ($\Omega_\ell, \Omega_{\Lambda_b}$ for Brane 1 and Brane 2). For the 'Gold' dataset, $y_i = \mu_{0,i} = m_B - M = 5\log d_L + 25$, the extinction corrected distance modulus for SNe at redshift z_i. The error $\sigma(\mu_{0,i})$ includes the uncertainty in galaxy redshifts due to a peculiar velocity of 400 km/s. For SNLS, $y_i = \mu_{B,i} = m_B - M + \alpha(s-1) - \beta c = 5\log_{10}(d_L/10\text{pc})$. The error $\sigma(\mu_{B,i})$ includes effects due to a peculiar velocity of 300 km/s. We assume a flat universe for our analysis.

We note that, for the SNLS data, we have to deal with two additional parameters α, β during the minimization. However, the error σ is dependent on α, β. Therefore, if we minimize with respect to all the parameters, the process will be biased towards increasing the errors in order to decrease the χ^2. To avoid this, we refrain from varying α, β together with the cosmological parameters. At each iteration α, β are fixed, while the remaining parameters are varied to obtain the minimum χ^2, then the values of α, β are changed for the next iteration. This process is continued till the global minimum is obtained. This method is equivalent to the method followed by the SNLS team, and for flat ΛCDM, our results concur with those in [8]. In presenting the final results, the nuisance parameters α, β, M (where M depends on H_0) are marginalized over to obtain bounds on the cosmological parameters of interest.

For Brane 1 and Brane 2, the cosmological parameters to be estimated are Ω_{0m}, Ω_ℓ and Ω_{Λ_b} (Ω_σ is calculated from Eqs (11) and (13) respectively for Brane 1 & Brane 2). After marginalizing over the statistical nuisance parameters, we obtain the three-dimensional probability distribution in the $(\Omega_{0m}, \Omega_\ell, \Omega_{\Lambda_b})$ space: $P(\Omega_{0m}, \Omega_\ell, \Omega_{\Lambda_b})$. We perform maximum likelihood analysis on the system with the priors $0 \leq \Omega_{0m} \leq 1$, $\Omega_\ell \geq 0$, $\Omega_{\Lambda_b} \geq 0$. For Brane 2, we use the added constraint $\Omega_\ell \leq 1 + \Omega_{\Lambda_b}$. For Brane 1 & Brane 2 the constraint relations (11), (13) combined with $\Omega_\kappa = 0$, set the lower bound $\Omega_{\Lambda_b} \geq -1$. However since $\Omega_{\Lambda_b} \geq 0$ is a more physically appealing model (it includes anti-de Sitter space (AdS) bulk geometry), we choose this as a prior for further analysis.

We may add further information to the analysis from the baryon acoustic oscillation (BAO) data. We obtain the joint probability distribution for the SNe data and the BAO data as $P(\chi^2_{SNe+BAO}) = P(\chi^2_{SNe})P(A)$, where A is the quantity defined in eq (3) and we assume that it follows a Gaussian probability distribution with mean $\bar{A} = 0.469$ and an error of $\sigma = 0.017$.

In the figure 1, we show the results for Brane 1 and Brane 2 using both Gold and SNLS data, in conjunction with the baryon acoustic oscillation peak (BAO). We show the reduced χ^2 per degrees of freedom as a function of Ω_{0m}, marginalized over $\Omega_\ell, \Omega_{\Lambda_b}, H_0$. For Brane 1, we find that the supernova data alone, in both cases, favours a somewhat larger value of Ω_{0m} at the minimum, with 'Gold' preferring a higher value than SNLS. When used in conjunction with BAO, however, both datasets prefer a matter density of $\Omega_{0m} \simeq 0.26$. For Brane 2, the preferred value of Ω_{0m} is around $\Omega_{0m} = 0.2$ for SNLS and around $\Omega_{0m} = 0.3$ for 'Gold'.

TABLE I: Best-fit $\Omega_{0m} - \Omega_\ell$ with corresponding 1σ errors for the Brane 1 model, with the present value of the equation of state w_0 and the best-fit χ^2 for the two supernova datasets. The best-fit χ^2 for ΛCDM is also shown for comparison.

	Ω_{0m}	Ω_ℓ	w_0	χ^2_{min}	$\chi^2_{\Lambda CDM}$
Gold+BAO	$0.274^{+0.039}_{-0.042}$	$0.0^{+0.031}$	$-1.0_{-0.057}$	1.13	1.13
SNLS+BAO	$0.269^{+0.041}_{-0.034}$	$0.054^{+0.051}_{-0.054}$	$-1.073^{+0.073}_{-0.035}$	1.08	1.15

TABLE II: Best-fit $\Omega_{0m} - \Omega_\ell$ with corresponding 1σ errors for the Brane 2 model, with the present value of the equation of state w_0 and the best-fit χ^2 for the two supernova datasets. The best-fit χ^2 for ΛCDM is also shown for comparison.

	Ω_{0m}	Ω_ℓ	w_0	χ^2_{min}	$\chi^2_{\Lambda CDM}$
Gold+BAO	$0.277^{+0.051}_{-0.038}$	$0.0^{+0.095}$	$-1.0^{+0.090}$	1.13	1.13
SNLS+BAO	$0.285^{+0.037}_{-0.036}$	$0.0^{+0.043}$	$-1.0^{+0.068}$	1.15	1.15

When used with BAO, once again, $\Omega_{0m} \simeq 0.26$ is preferred.

During the analysis we find that for both Brane 1 and Brane 2, the results are very weakly dependent on the bulk cosmological constant Ω_{Λ_b}, and marginalizing over Ω_{Λ_b} does not affect the results very much. In further analysis, we therefore fix the value of Ω_{Λ_b} to its best-fit value of $\Omega_{\Lambda_b} = 0$.

In the table I we show the best-fit $\Omega_{0m} - \Omega_\ell$ with 1σ errors around it for the Brane 1 model for the two supernova datasets, with the χ^2 at the best-fit. The best-fit χ^2 for ΛCDM is also shown for comparison. We know that the supernova data alone is not able to place strong constraints on the value of the matter density Ω_{0m} for Brane 1 models for both datasets (see upper panel of figure 3). If we use the baryon acoustic oscillation peak in conjunction with the supernova data, then there are stringent and realistic constraints on the value of Ω_{0m}, therefore we show the χ^2 for the joint probability distribution only. For the Brane 1 model, Ω_ℓ cannot be negative, and $w_0 \leq -1$ always, and we show the bounds on Ω_ℓ and w_0 accordingly. For the Gold dataset, the supernova and BAO data in conjunction favour a ΛCDM universe with $\Omega_{0m} = 0.274^{+0.039}_{-0.042}$ and $\Omega_\ell = 0.0^{+0.031}$. The "effective" equation of state at present is $w_0 = -1.0_{-0.057}$. For the SNLS dataset, a braneworld model with a small value of Ω_ℓ is slightly favoured over ΛCDM, with $\Omega_{0m} = 0.269^{+0.041}_{-0.034}$ and $\Omega_\ell = 0.054^{+0.051}_{-0.054}$. The present value of the "effective" equation of state is $w_0 = -1.073^{+0.073}_{-0.035}$. Since $\Omega_\ell = 0$
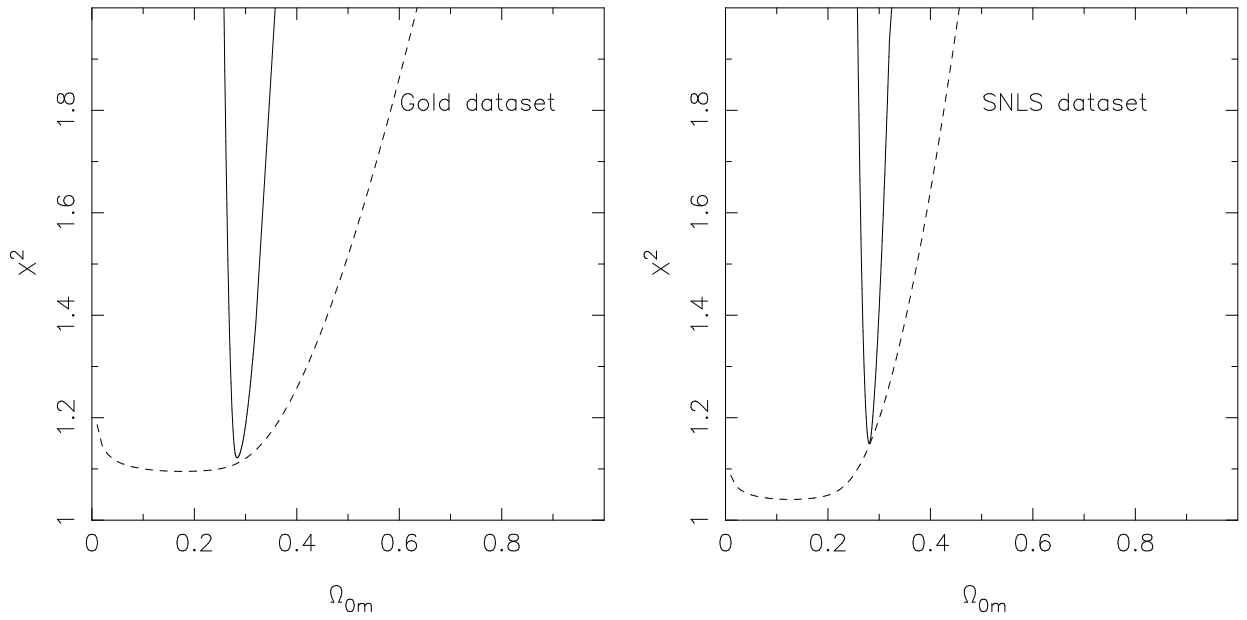
Brane 1
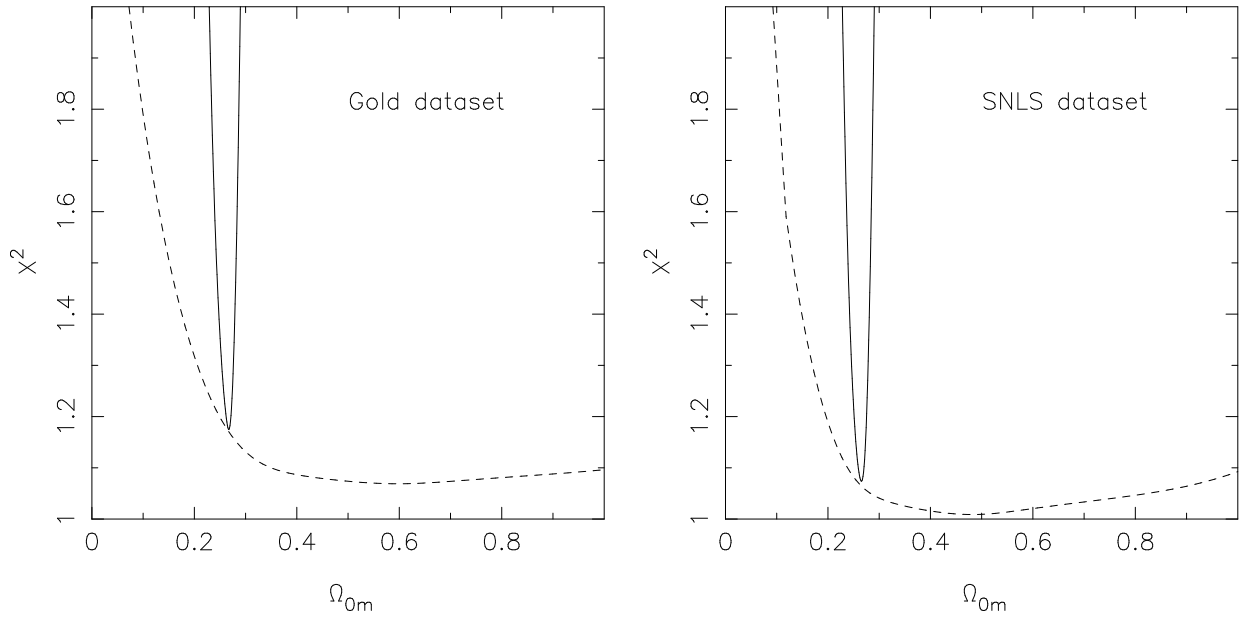
Brane 2

FIG. 1: The reduced χ^2 per degree of freedom as a function of Ω_{0m}, marginalized over $\Omega_\ell, \Omega_{\Lambda_b}, H_0$ for Brane 1 (top) and Brane 2 (bottom). The left panel shows results for the Gold Supernova data while the right panel shows results for the SNLS data. The dashed line is each panel is obtained by using supernova data alone, while the solid line uses both SNe data and the baryon oscillation peak.
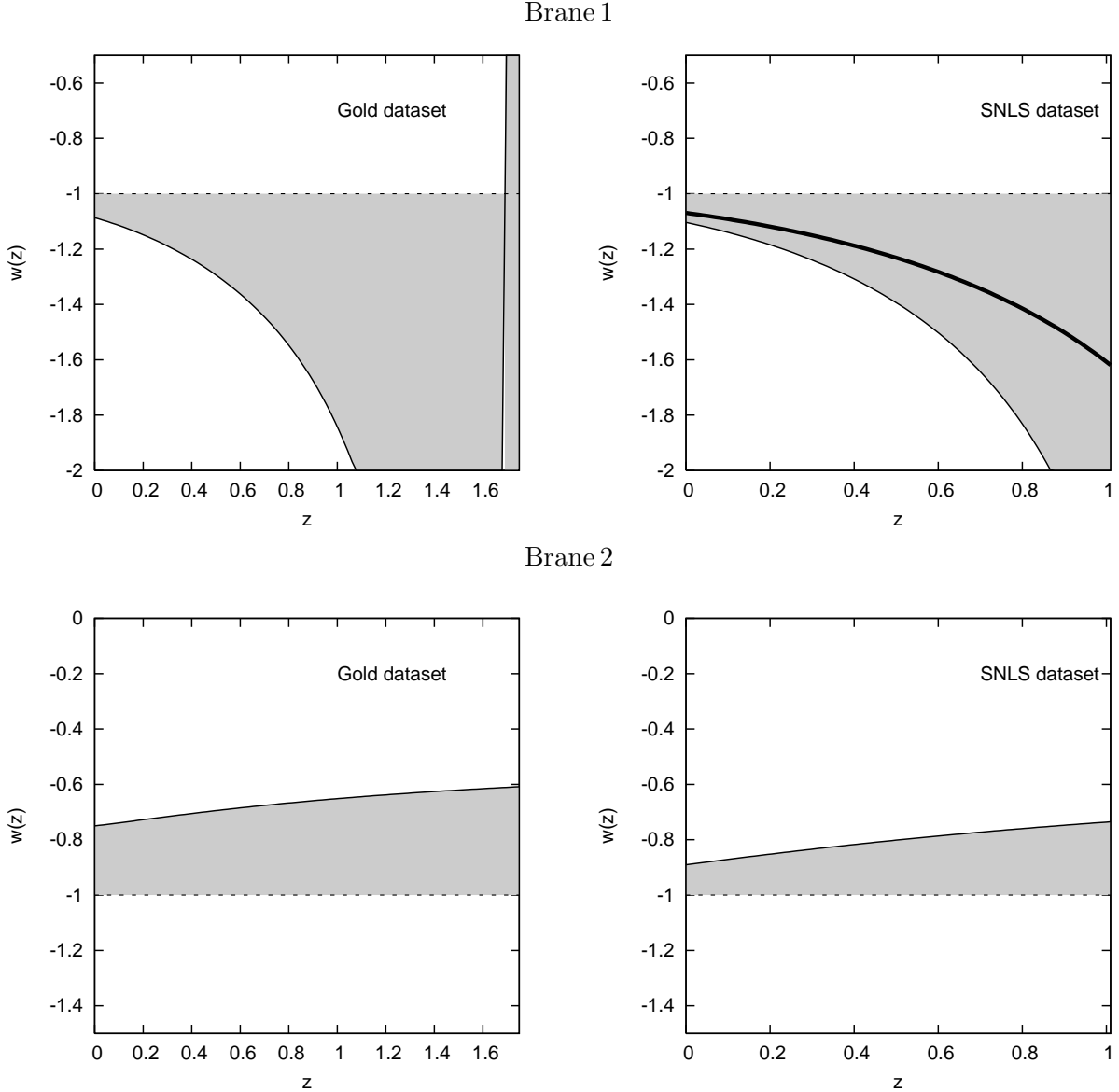
FIG. 2: The redshift variation of the "effective" equation of state $w(z)$ for the Brane 1 (top panel) and Brane 2 (bottom panel) models using the Gold+BAO (left panel) and SNLS+BAO (right panel) datasets. The light grey contours denote the 1σ errors around the best-fit, and the dashed line represents ΛCDM, which is the upper (lower) limit for $w(z)$ for the Brane 1 (Brane 2) model. In the top right panel, the thick solid line represents the best-fit for the SNLS+BAO data for the Brane 1 model. For the other three cases, the best-fit is at the ΛCDM line. We see that the behaviour of the "effective" equation of state of the braneworld models can be markedly different from ΛCDM within 1σ even for the small values of Ω_ℓ allowed by the data, especially for Brane 1. For the Gold data, which extends to higher redshifts, we can even see the existence of a pole in the "effective" equation of state for the Brane 1 models.

13

represents ΛCDM, this implies that BAO and SNe data together choose a best-fit Brane 1 model that is either equivalent to, or very close to, the ΛCDM model. However, within 1σ, the value of Ω_ℓ allowed is sufficiently large to allow for interesting braneworld behavior, especially for the SNLS data.

In the table II, we similarly show the best-fit $\Omega_{0m} - \Omega_\ell$ with 1σ errors around it for the Brane 2 model for the two supernova datasets, with the χ^2 at the best-fit, along with the best-fit for ΛCDM. As before, since for the Brane 2 model, Ω_ℓ cannot be negative, and $w_0 \geq -1$ always, we show the bounds on Ω_ℓ and w_0 accordingly. In this case, the current data appears to favour a ΛCDM universe over the Brane 2 model for both datasets. Somewhat larger values of Ω_ℓ are allowed for Brane 2 within 1σ for the Gold data than for the SNLS data.

The low values of Ω_ℓ allowed by the current data for both the braneworld models can still give rise to sufficiently interesting behaviour. To demonstrate this, in figure 2 we show the 1σ confidence levels for the "effective" equation of state w for the Brane 1 and Brane 2 models using Gold+BAO and SNLS+BAO data. We see that, even for the small values of Ω_ℓ allowed by the data, the "effective" equation of state looks quite different from the $w = -1$ cosmological constant model within 1σ especially for the Brane 1 model. In fact, for the Gold data, which extends to higher redshifts, we can see the existence of a singularity in the "effective" equation of state at $z \simeq 1.6$ for the Brane 1 model. We would like to emphasize here that the presence of such poles in the "effective" quantity $w(z)$ does not signal to any inherent pathologies of the braneworld models described here, since the scale factor and its derivatives remain well behaved throughout the evolution of the universe. Indeed, the reason for the occurance of a pole is simple and has to do with the fact that the density parameter $\Omega_m(z)$, which increases with increasing redshift, crosses unity at high z [22, 24]. This results in a pole in the effective equation of state, since $w(z)$ in (15) diverges when $\Omega_m(z) \to 1$. It should be stressed that the diverging equation of state is a signature of these braneworld models. Although it is difficult to reconstruct a diverging equation of state using standard parametrizations of dark energy, the equation of state of such braneworld models can be successfully reconstructed using other reconstruction techniques such as smoothing of the supernova data [34]. So, it is hoped that with better quality data, it should be possible to test braneworld models by studying the behaviour of the effective equation of state at high z. At present we see that, within 1σ, braneworld models that are distinctly different

from the cosmological constant are able to satisfy the current supernova data and therefore remain a possible candidate for dark energy along with the cosmological constant.

In figure 3, we further explore the $\Omega_{0m} - \Omega_\ell$ parameter space for the Brane 1 and Brane 2 models. We see from the $1\sigma, 2\sigma, 3\sigma$ contours that Brane 1 satisfies the SNLS dataset for a larger region in the $\Omega_{0m} - \Omega_\ell$ parameter space as compared to the Gold dataset. BAO does not depend very strongly on the value of Ω_ℓ, rather, it is sensitive to the value of Ω_{0m}. Therefore, in conjunction with BAO, Brane 1 provides a better fit to the SNLS data than to the Gold data. The situation is just the opposite in the case of Brane 2, which provides a better fit to the Gold data as compared to the SNLS data.

An interesting feature of braneworld models is that for a finite region of parameter space, the Brane 2 universe can expand towards a 'quiescent' future singularity at which the energy density and the Hubble parameter remain well behaved, but higher derivatives of the expansion factor ($\ddot{a}$, $\dddot{a}$ etc.) diverge [35]. From (12) we see that a braneworld model which satisfies

$$\Omega_\sigma + \Omega_\ell + \Omega_{\Lambda_b} < 0. \tag{23}$$

will run into a future singularity at the redshift

$$z_s = \left(-\frac{\Omega_\sigma + \Omega_\ell + \Omega_{\Lambda_b}}{\Omega_{0m}}\right)^{1/3} - 1 . \tag{24}$$

The time of occurrence of the singularity (measured from the present moment) can easily be determined from

$$T_s = t(z = z_s) - t(z = 0) = \int_{z_s}^0 \frac{dz}{(1+z)H(z)}, \tag{25}$$

where $H(z)$ is given by (12).

From the lower panel of figure 3, we see that universes which terminates in a 'quiescent' future singularity are excluded at the 3σ confidence level for both SNLS and Gold datasets when used in conjunction with the baryon oscillations.

As noted in section , the DGP model forms a special case of our braneworld cosmology obtained by putting $\Omega_{\Lambda_b} = \Omega_\sigma = 0$ in equation 12. We see that using the SNLS data together with BAO, we may narrowly rule out the DGP model of braneworld dark energy at 3σ (thick solid line in right lower panel of figure 3). However, for the Gold data and BAO, the flat DGP model is acceptable within 2σ (thick solid line in left lower panel of figure 3)[42].
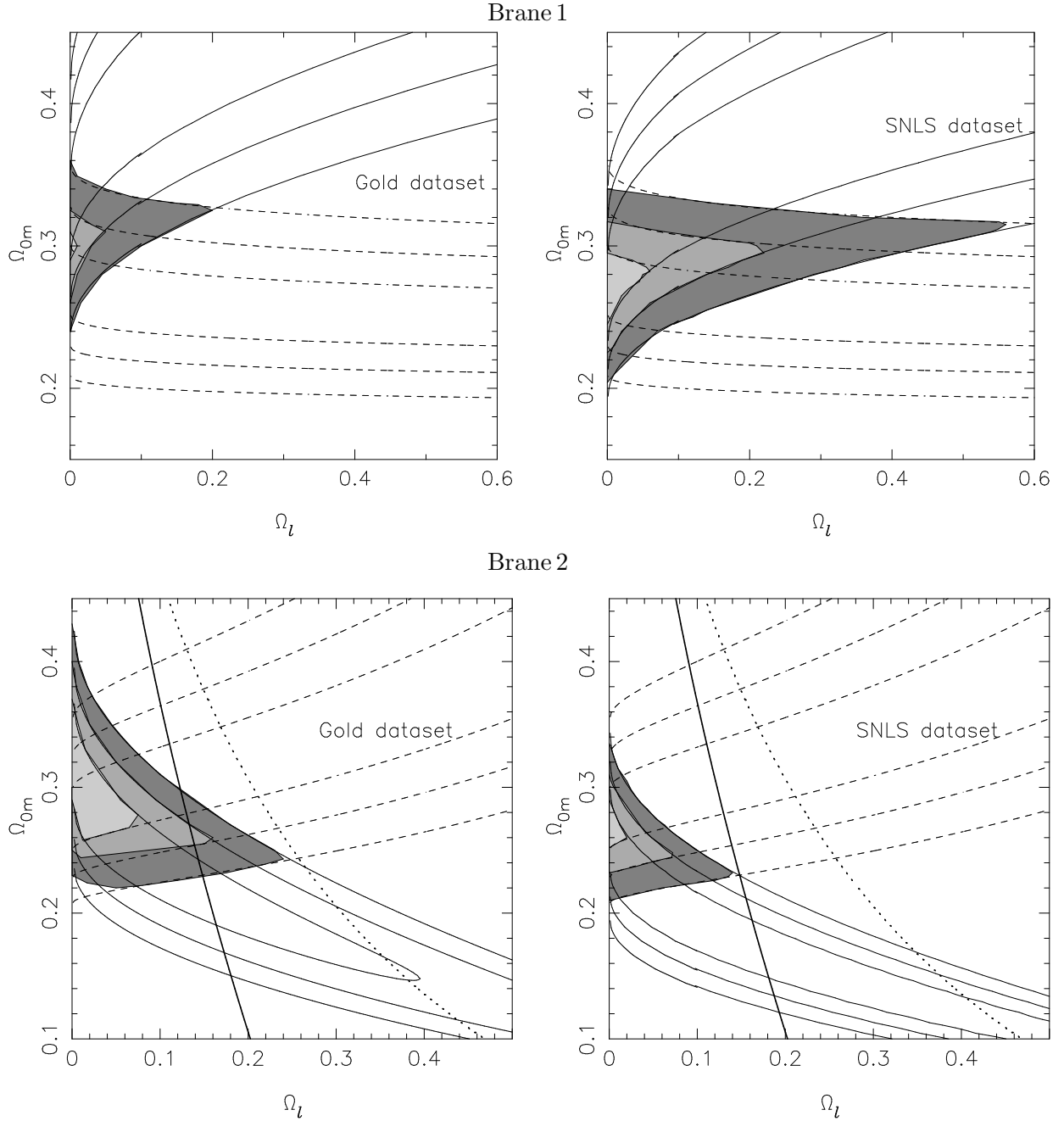
Brane 1

Brane 2

FIG. 3: Confidence levels in the $\Omega_{0m} - \Omega_\ell$ plane for Brane 1 (top) and Brane 2 (bottom). H_0 is marginalized over and Ω_{Λ_b} is fixed at the best fit value of $\Omega_{\Lambda_b} = 0$. The left panel shows results for the Gold Supernova data while the right panel shows results for the SNLS data. The solid lines in each panel represent the $1, 2, 3\sigma$ confidence levels obtained by using supernova data alone, while the dashed lines are the $1, 2, 3\sigma$ contours for the baryon oscillation peak. The light grey, medium grey and dark grey contours represent the $1, 2, 3\sigma$ confidence levels when the supernova data is used in conjunction with the baryon oscillation peak. The region to the right of the thick dotted line in the lower panels represents Brane 2 models which will undergo a future 'quiescent' singularity. The thick solid line in the lower panels represents the DGP model.

We therefore conclude that while the flat Brane 1 and Brane 2 models are able to satisfy the Gold and SNLS data data over a reasonable region of parameter space, both the DGP model and the model with a quiescent future singularity are in tension with the data. For both the supernova datasets, the more general flat Brane 1 and Brane 2 models are able to satisfy the data over a reasonable region of parameter space.

CONCLUSIONS

We have demonstrated that high redshift type Ia supernova data [7, 9] when combined with the recent discovery of baryon oscillations in the SDSS [30] can serve to place significant constraints on the parameter space of braneworld models.

Our results for the Gold data set are in broad agreement with the earlier work of [36] who tested braneworld models against an early SNe data set (also see [37]). Our results for the Supernova Legacy Survey (SNLS) are in good agreement with those of [38] who recently tested the DGP model using SNLS and baryon oscillations. Since the DGP model forms a subset of the braneworld models analyzed by us we find that the SNLS data together with baryon oscillations rule out this model at 3 σ. However we also find that the DGP model is more strongly constrained by SNLS than by the Gold data set of [7], which allows the DGP model at 2σ. Our analysis also shows that baryon oscillations in conjunction with SNe data rule out a class of braneworld models in which the universe encounters a 'quiescent' future singularity where the density, pressure and Hubble parameter remain finite but higher derivatives of the scale factor diverge.

Our analysis indicates that the Gold and SNLS supernovae place slightly different constraints on the braneworld parameters. Thus although figures 1, 3 clearly show that the Braneworld models analyzed by us agree well with both sets of SNe data, the Gold data set accommodates larger values of $\Omega_{0m} \gtrsim 0.25$ than SNLS ($\Omega_{0m} \gtrsim 0.2$) for the Brane 1 model. In the case of Brane 2 smaller values $\Omega_{0m} \lesssim 0.35$ appear to be favoured by SNLS than by Gold ($\Omega_{0m} \lesssim 0.45$). Thus Brane 1 models fit better to the SNLS data, while Brane 2 models fit better to the Gold dataset.

In this connection it is interesting to note that the recent analysis of evolving dark energy models using Gold and SNLS data [39] found somewhat different trends in the evolution of dark energy favoured by these two data sets. It is hoped that improvements in the quality

and quantity of future SNe data will allow tighter constraints to be placed on dark energy models. We would like to draw attention to the fact that in this paper we have explored the region of parameter space in which $\Omega_{\Lambda_\text{b}}$ is reasonably small. The reason for this is that performing a likelihood analysis for the full (formally infinite) region of parameter space is computationally very expensive and so we have restricted our analysis to a finite region of parameter space corresponding to $\Omega_{\Lambda_\text{b}} \lesssim 1$, $\Omega_\ell \lesssim 1$ which includes ΛCDM and the DGP braneworld as subclasses. In this context it is interesting to note that braneworld models with fundamentally new properties can arise for large values of $\Omega_{\Lambda_\text{b}} \gg 1$. For instance, the mimicry model briefly touched upon in section II, mimics ΛCDM at low redshifts while departing from the latter at higher redshifts. The presence of a 'dark radiation' term (which quantifies the projection of higher dimensional 'bulk' effects on to the brane) allows for even more radical departures from standard cosmology by permitting the universe to 'loiter' at moderately large redshifts $1 \ll z \ll 1000$. Both 'loitering' [24] and 'mimicry' [25] models predict a lower redshift of reionization and a longer age for QSO's and other high redshift objects when compared with ΛCDM. However at low z both models remain very close to ΛCDM and for this reason are unlikely to be distinguished from the latter on the basis of SNe data alone. For this reason we have not included 'loitering' and 'mimicry' models into the present analysis but hope to return to these models in a companion paper.

Acknowledgments

[1] Perlmutter, S.J. et al., Nature **391**, 51 (1998).

[2] Riess, A.G. et al., Astron. J. **116**, 1009 (1998).

[3] Perlmutter, S.J. et al., Astrophys. J. **517**, 565 (1999).

[4] Tonry, J.L., et al., 2003, Astrophys. J. **594**, 1, [astro-ph/0305008].

[5] Knop, R.A., *et al.*, Astrophys.J. **598**, 102, (2003) [astro-ph/0309368].

[6] Barris, B. J. *et al.*, Astrophys.J. **602**, 571 (2004) [astro-ph/0310843].

[7] Riess, A.G. *et al.*, Astrophys.J. **607**, 665 (2005) [astro-ph/0402512]

[8] Howell, D.A., for the SNLS Collaboration, 2004, To appear in "1604-2004: Supernovae as Cosmological Lighthouses", Padua, June 16-19 2004, eds. Turatto et al., ASP conference Series.

[9] Astier, P. *et al.*, *The Supernova Legacy Survey: Measurement of* Ω_{M}, Ω_{Λ} *and w from the First Year Data Set*, astro-ph/0510447.

[10] Spergel, D.N., et al, Astrophys.J.Suppl. **148**, 175 (2003) [astro-ph/0302209]

[11] Tegmark, M. et al, Phys. Rev. D **69**, 103501 (2004) [astro-ph/0310723]

[12] Sahni, V. and Starobinsky, A.A. *IJMP D* **9**, 373 (2000) [astro-ph/9904398]; Carroll, S.M., Living Rev.Rel. **4** 1 (2001) [astro-ph/0004075]; Peebles, P.J.E. and Ratra, B., Rev.Mod.Phys. **75**, 559 (2002). [astro-ph/0207347]; Padmanabhan, T., Phys. Rep. **380**, 235 (2003). [hep-th/0212290]; Sahni, V. *Dark Matter and Dark Energy*, Lectures given at the 2nd Aegean Summer School on the Early Universe, Ermoupoli, Island of Syros, Greece, astro-ph/0403324; Sahni V, *Cosmological surprises from Braneworld models of dark energy*, astro-ph/0502032.

[13] Weinberg, S., Rev. Mod. Phys. **61**, 1 (1989).

[14] Horava, P. and Witten, E. Nucl. Phys. **B 460**, 606 (1996); Nucl. Phys. **B 475**, 94 (1996).

[15] Randall, L. and Sundrum, R., Phys. Rev. Lett. **83**, 3370 (1999), [hep-ph/9905221]; L. Randall and R. Sundrum, Phys. Rev. Lett. **83**, 4690 (1999), [hep-th/9906064].

[16] Maartens A, 2004 *Living Rev. Rel.* **7** 7 [gr-qc/0312059]

[17] Peebles, P.J.E. and Vilenkin, A., Phys. Rev. D **59**, 063505 (1999).

[18] Copeland, E.J., Liddle, A.R. and Lidsey, J.E. Phys. Rev. D **64** 023509 (2001); Huey, G. Huey Lidsey, J. Phys. Lett. B **514**, 217 (2001); Sahni, V., Sami, M. and Souradeep, T., Phys. Rev. D **65** 023518 (2002); Majumdar, A. S. Phys. Rev. D **64**, 083503 (2001); Feng, B. and Li, M., Phys.Lett., **B** 564, 169 (2003) [hep-ph/0212213]; Liddle, A. R. and Urena-Lopez, L.A., Phys. Rev. D **68**, 043517 (2003) [astro-ph/0302054]; Dimopoulos, K., Phys. Rev. D **68**, 123506 (2003) [astro-ph/0212264]; Shiromizu,, T., Torii, T. and Uesugi, T., Phys. Rev. D 67, 123517 (2003) [hep-th/0302223]; Sami, M., Dadhich, N. and Shiromizu, T., Phys.Lett. B **568** 118 (2003) [hep-th/0304187]; Sami, M. and Sahni, V., Phys. Rev. D **D70** 083513 (2004) [hep-th/0402086].

[19] Dvali, D, Gabadadze, G and Porrati, M, 2000 *Phys. Lett.* B **485** 208 [hep-th/0005016].

[20] Deffayet, C, Dvali, G, and Gabadadze, G, Phys. Rev. D **65**, 044023 (2002) [astro-ph/0105068]; Deffayet,C, Landau, S.J., Raux, J., Zaldarriaga, M., and Astier, P., Phys. Rev. D **66**, 024019

(2002). [astro-ph/0201164].

[21] Sakharov,A. D. Dokl. Akad. Nauk SSSR. Ser. Fiz. **177**, 70 (1967) [Sov. Phys. Dokl. **12**, 1040 (1968)]; reprinted in: Usp. Fiz. Nauk **161**, 64 (1991) [Sov. Phys. Usp. **34**, 394 (1991)]; Gen. Rel. Grav. **32**, 365 (2000).

[22] Sahni, V. and Shtanov, Yu.V., JCAP 0311,014, (2003) [astro-ph/0202346].

[23] Fischler, W., A. Kashani-Poor, R. McNees, and S. Paban, JHEP **0107**, 3 (2001) [hep-th/0104181]; J. Ellis, N. E. Mavromatos, and Nanopoulos, D. V. *String theory and an accelerating universe*, hep-th/0105206; J. M. Cline, JHEP **0108**, 35 (2001) [hep-ph/0105251]; X.-G. He, *Accelerating universe and event horizon*, `astro-ph/0105005`.

[24] Sahni V and Shtanov Yu, Phys. Rev. D **71** 084018 (2005) [astro-ph/0410221]

[25] Sahni V and Shtanov Yu and Viznyuk, A., *Cosmic Mimicry: Is LCDM a Braneworld in disguise ?* astro-ph/0505004.

[26] Richards G T *et al.*, *Astron. J.* **127** 1305 (2004) [astro-ph/0309274]

[27] Haiman Z and Quataert E, *The Formation and Evolution of the First Massive Black Holes*, 2004, astro-ph/0403225.

[28] Barkana R and Loeb A, *In the Beginning: The First Sources of Light and the Reionization of the universe*, astro-ph/0010468; Ciardi B and Ferrara A, *The First Cosmic Structures and their Effects*, astro-ph/0409018; O. Elgaroy, D.F. Mota and T. Multamaki, Phys. Rev. D **D71**, 067301 (2005) [astro-ph/0501342].

[29] Friaca, A., Alcaniz, J.S. and Lima, J.A.S., MNRAS **362** 1295 (2005) [astro-ph/0504031]; Jain, D. and Dev, A., *Age of High Redshift Objects - a Litmus Test for the Dark Energy Models*, astro-ph/0509212.

[30] Eisenstein, D.J. *et al.*, *Detection of the Baryon Acoustic Peak in the Large-Scale Correlation Function of SDSS Luminous Red Galaxies*, Astrophys. J. **633**, 560 (2005) [astro-ph/0501171].

[31] Collins, H. and Holdom, B., Phys. Rev. D **62**, 105009 (2000) [hep-ph/0003173].

[32] Shtanov,Yu. V., *On brane-world cosmology*, hep-th/0005193.

[33] Lue, A. and Starkmann, G.D., Phys. Rev. D **D70**, 101501 (2004) [astro-ph/0408246].

[34] Shafieloo, A., Alam, U., Sahni, V. and Starobinsky, A. A., *Smoothing Supernova Data to Reconstruct the Expansion History of the Universe and its Age*, Mon. Not.@ Roy. Ast. Soc. **366** 1081 (2006) [astro-ph/0505329].

[35] Yu. Shtanov and V. Sahni, Class.Quant.Grav. **19**, L101 (2002) [gr-qc/0204040].

[36] Alam U and Sahni V, *Supernova Constraints on Braneworld Dark Energy*, astro-ph/0209443.

[37] Szydlowski, M. and W. Godlowski, W., *Can brane dark energy model be probed observationally by distant supernovae?* astro-ph/0511259.

[38] Fairbairn, M. and Goobar, A., *Supernova limits on brane world cosmology*, astro-ph/0511029.

[39] Nesseris, S. and Perivolaropoulos, L., *Comparison of the Legacy and Gold SnIa Dataset Constraints on Dark Energy Models*, astro-ph/0511040.

[40] We have neglected the dark radiation term for simplicity.

[41] It is interesting to note that Brane 1 models have $w_0 \leq -1$ and $w(z) \simeq -0.5$ at $z \gg 1$. They therefore successfully cross the 'phantom divide' at $w = -1$.

[42] Similar results have also been independently obtained by Roy Maartens and Elisabetta Majerotto (private communication).